

# Potassium and soot interaction in fast biomass pyrolysis at high temperatures

Anna Trubetskaya<sup>a,\*</sup>, Flemming Hofmann Larsen<sup>b</sup>, Andrey Shchukarev<sup>c</sup>,  
Kenny Ståhl<sup>d</sup>, Kentaro Umeki<sup>e</sup>

<sup>a</sup>*Thermochemical Energy Conversion Laboratory, Umeå University, 90187 Umeå, Sweden*

<sup>b</sup>*Department of Food Science, University of Copenhagen, Rolighedsvej 26, 1958  
Copenhagen, Denmark*

<sup>c</sup>*Department of Chemistry, Umeå University, 90187 Umeå, Sweden*

<sup>d</sup>*Department of Chemistry, Technical University of Denmark, Kemitorvet B206, 2800  
Kongens Lyngby, Denmark*

<sup>e</sup>*Energy Science Division, Luleå University of Technology, 97187 Luleå, Sweden*

---

## Abstract

This study aims to investigate the interaction between potassium and carbonaceous matrix of soot produced from wood and herbaceous biomass pyrolysis at high heating rates at 1250°C in a drop tube reactor. The influence of soot carbon chemistry and potassium content in the original biomass on the CO<sub>2</sub> reactivity was studied by thermogravimetric analysis. The XPS results showed that potassium incorporation with oxygen-containing surface groups in the soot matrix did not occur during high temperature pyrolysis. The potassium was mostly found as water-soluble salts such as KCl, KOH, KHCO<sub>3</sub> and K<sub>2</sub>CO<sub>3</sub> in herbaceous biomass soot. The low ash-containing pinewood soot was less reactive than the potassium rich herbaceous biomass soot, indicating a dominating role of potassium on the soot reactivity. However, the catalytic effect of potassium on the reactivity remained the same

---

\*Corresponding author. anna.trubetskaya@umu.se

after a certain potassium amount was incorporated in the soot matrix during pyrolysis. Raman spectroscopy results showed that the carbon chemistry of biomass soot also affected the CO<sub>2</sub> reactivity. The less reactive pinewood soot was more graphitic than herbaceous biomass soot samples with the disordered carbon structure.

*Keywords:* soot, potassium, biomass, fast pyrolysis, CO<sub>2</sub> reactivity

---

## 1. Introduction

Entrained flow gasification (EFG) is a promising technology, which generates high quality syngas and small amounts of tars due to the high operating temperatures. However, the high soot yields lead to intensive gas cleaning and can cause a possible plant shut down. The reduction of soot formation increases the overall production system efficiency and improves the economic feasibility and reliability of the gasification plant. Moreover, the alkali metals released from high ash-containing lignocellulosic materials may form molten ash material, and thus, lead to deposition of slag upon the reactor wall [1, 2]. Continuous extraction of the ash slag from the reactor is required to prevent outlet blockages and to ensure steady syngas production.

The released alkali metal ions in the biomass pyrolysis participate in soot formation and conversion reactions. It is known that alkali metal ions enhance CO<sub>2</sub> reactivity of graphite and carbon black [3] and suppress soot formation [4]. The alkali metal ions can form a fly ash or be bonded to oxygen-containing surface groups in the soot matrix [5, 6]. The fly ash particles contain K<sub>2</sub>S, KOH and K<sub>2</sub>CO<sub>3</sub> [6]. The interaction of K<sub>2</sub>CO<sub>3</sub> with the low ash-containing coal was investigated under CO<sub>2</sub> gasification condition in

19 a thermogravimetric analyzer by Kopyscinski et al. [7]. The pyrolysis results  
20 showed that CO was released from  $K_2CO_3$ , which was bound to a carbon sur-  
21 face. In the next step, the oxygen from the carbonate reacts further with the  
22 surface carbon and forms CO which leaves the reduced potassium complex  
23 of an unknown stoichiometry. In the last step, the transfer of the potassium  
24 cluster occurs. During fast pyrolysis, the elemental potassium is unlikely  
25 to be released in gas phase at low temperatures. However, little is known  
26 about the interaction between the carbonaceous matrix of soot and alkali. In  
27 catalytic gasification, the concentration of intercalated species is small, and  
28 it decreases with increasing temperature [8, 9]. The elemental potassium,  
29 bonded to the soot matrix in phenolate groups remained inaccessible for the  
30 gaseous reactants, leading to the low catalytic activity [10]. The potassium-  
31 carbon complexes form a series of stable and metastable phases with different  
32 physicochemical properties [11–14]. The K- $C_{60}$  complex was investigated us-  
33 ing  $^{13}C$  and  $^{39}K$  solid state NMR [15]. According to the  $^{13}C$  NMR spectra  
34 of intercalated graphite ( $K_1C_{60}$ ) it exists as a single phase characterized by  
35 a resonance at 174 ppm at temperatures above 420 K [13]. At lower tem-  
36 peratures, two resonances of intercalated graphite at 187 ppm ( $K_3C_{60}$ ) and  
37 143 ppm ( $K_\delta C_{60}$ ,  $\delta \leq 1$ ) were identified by  $^{13}C$  NMR [13]. X-ray photoelec-  
38 tron spectrum of potassium doped double-walled carbon nanotubes showed  
39 two peak components at the binding energy of 293.3 and 296 eV (K  $2p_{3/2}$  and  
40 K  $2p_{1/2}$  of the K-oxides and K-cations) [16]. The X-ray photoelectron bands  
41 at 294.6 and 293.4 eV were assigned to ionic potassium intercalated within  
42 the graphite layers and to oxidized potassium at the surface of graphite [17].  
43 The modeling using density functional theory method (DFT) confirmed the

44 existence of an electron transfer from soot to gaseous oxygen through the  
45 active  $K^+$  sites [18]. In this DFT model, soot structure was represented by  
46 graphene layers and potassium was modeled perpendicular to the plane of the  
47 soot model and near the zigzag and armchair edges of the soot. The DFT  
48 model for the C-C armchair face showed that the potassium intercalation  
49 in phenolate groups (C-O-K) inhibits the gasification reaction, confirming  
50 previous experimental observations [3, 19].

51 This work aims to investigate the interaction between potassium and  
52 carbonaceous soot matrix in detail. The specific objectives of this study  
53 were to: (1) investigate the interaction of potassium with the carbonaceous  
54 matrix of soot produced at high temperatures (1250°C) in a drop tube re-  
55 actor, and (2) understand the formation mechanism of potassium-carbon  
56 complexes in fast pyrolysis and their effect on the soot reactivity using Ra-  
57 man spectroscopy, X-ray photoelectron spectroscopy (XPS),  $^{13}C$  solid state  
58 NMR, X-ray diffraction (XRD), and thermogravimetric analysis (TGA).

## 59 **2. Materials and methods**

### 60 *2.1. Raw biomass characterization*

61 Pinewood, beechwood, wheat straw and alfalfa straw were chosen for  
62 the fast pyrolysis study in a drop tube reactor (DTF). Fuel selection was  
63 based on the differences in the ash composition and plant cell compounds  
64 (cellulose, hemicellulose, lignin, extractives), as shown in the supplemental  
65 material (Table S-1). The ultimate and proximate analysis of pinewood,  
66 beechwood, wheat straw, leached wheat straw and alfalfa straw is shown in  
67 Table 1.

Table 1: Proximate and ultimate analysis.

Fuel	Pinewood	Beechwood	Wheat straw	Alfalfa straw	Leached wheat straw
Proximate analysis					
Moisture, (wt. % as received)	5.1	4.5	5.5	5.2	4.3
Ash (550°C), (wt. % dry basis)	0.3	1.4	4.1	7.4	2.1
Volatiles, (wt. % dry basis)	86.6	79.4	77.5	75.9	82.2
HHV, (MJ kg <sup>-1</sup> )	21.6	20.2	18.8	19.7	19
LHV, (MJ kg <sup>-1</sup> )	20.2	19	17.5	16.9	17.2
Ultimate analysis, (wt. %, dry basis)					
C	53.1	50.7	46.6	42.5	46.2
H	6.5	5.9	6.1	6.7	6.8
O	40	41.9	42.5	43.1	44.9
N	0.06	0.13	0.6	0.3	0.05
S	< 0.01	0.01	0.1	0.03	0.02
Ash compositional analysis, (mg kg <sup>-1</sup> , dry basis)					
Cl	0.01	0.02	0.1	0.5	0.01
Al	10	10	150	600	100
Ca	600	2000	2500	12900	1300
Fe	20	10	200	-	350
K	200	3600	11000	28000	1200
Mg	100	600	750	1400	350
Na	30	100	150	1000	50
P	6	150	550	1900	80
Si	50	200	8500	2000	6200
Ti	2	< 8	10	30	10

68 *2.2. Pyrolysis with drop tube furnace*

69 Soot and char samples were obtained from pyrolysis experiments in a  
70 drop tube reactor (DTF). Soot samples were generated at 1250°C to ob-  
71 tain a maximal soot yield. The DTF setup and operating conditions were  
72 described in detail by Trubetskaya et al. [20]. The reactor consists of an

73 alumina tube (internal diameter: 54 mm, heated length: 1.06 m) heated by  
74 four heating elements with independent temperature control. Gas flow rate  
75 into the reactor is regulated by mass flow controllers (EL-FLOW<sup>®</sup> Select,  
76 Bronkhorst High-Tech B.V.). The experiments were conducted by feeding  $\approx$   
77 5 g of biomass at a rate of  $0.2 \text{ g min}^{-1}$ . Both primary ( $0.181 \text{ min}^{-1}$  measured  
78 at  $20^\circ\text{C}$  and  $101.3 \text{ kPa}$ ) and secondary ( $4.81 \text{ min}^{-1}$  measured at  $20^\circ\text{C}$  and  
79  $101.3 \text{ kPa}$ ) feed gases were  $\text{N}_2$ . The residence time of fuel particles was esti-  
80 mated to be about 1 s, taking into account density changes during pyrolysis.  
81 Soot particles passing the cyclone (cut size  $2.5 \mu\text{m}$ ) were captured from the  
82 product gas flow by a grade QM-A quartz filter with a diameter of 50 mm  
83 (Whatman, GE Healthcare Life Science).

### 84 *2.3. Solid residue characterization*

85 *Ash compositional analysis.* The ash compositional analysis was performed  
86 by ICP-OES (DIN EN 15290). Prior to the analysis, soot samples were pre-  
87 heated in oxygen at  $10^\circ\text{C min}^{-1}$  up to  $550^\circ\text{C}$  and kept at that temperature  
88 for 7 h.

89 *Potassium ion selective electrode.* The potassium ion-selective membrane elec-  
90 trode Orion 93-19 (Thermo Scientific, USA) was used to determine the  
91 amount of leached potassium in deionized water. The electrode potential  
92 was measured at room temperature using the Benchtop Meter Orion 720A  
93 (Thermo Scientific, USA). Five-points calibration was conducted using potas-  
94 sium chloride solutions with ionic strengths of  $10^{-5}$ ,  $10^{-4}$ ,  $10^{-3}$ , 0.01 and  
95 0.1 M.

96 *X-ray diffraction.* The XRD analysis of the soot matter was conducted using  
97 a Bruker D8 AXS X-ray diffractometer with (Cu-K $\alpha$ 1,  $\lambda = 1.54056 \text{ \AA}$  and  
98 Cu-K $\alpha$ 2 radiation,  $\lambda = 1.54439 \text{ \AA}$ ) operating in Bragg-Brentano (reflection)  
99 mode, using a secondary graphite monochromator, and a scintillation de-  
100 tector, in the range 5 to 80 degrees for 12.5 h. Soot samples were placed in  
101 small cups which were rotated during the XRD analysis. The multiple fitting  
102 of XRD pattern, crystallite size analysis and peak searches were done using  
103 PowderPlot software and Crystallographica Search-Match software (Version  
104 3,1,0,0). The instrumental reflection broadening was subtracted from the  
105 experimental pattern by the PowderPlot software.

106 *Raman spectroscopy.* Raman spectroscopy was performed using an inVia Ra-  
107 man microscope (Renishaw, UK) operating with a 514 nm laser line at a  
108 power of 30 mW. The measurements were performed in static mode with a  
109 centre at  $1600 \text{ cm}^{-1}$  resulting in a  $960\text{-}2200 \text{ cm}^{-1}$  spectral region. The laser  
110 power was set to 100 % in the software and roughly 30 % in the hardware.  
111 1 s exposure time was used in normal confocality mode. A 20x lens and  
112  $8\text{-}15 \mu\text{m}$  step size (X and Y directions) were used for mapping, to generate  
113 100-200 spectra/image for each soot sample. Deconvolution of the Raman  
114 spectra were conducted using the peak fit pro tool in the OriginPro software  
115 (OriginLab, USA) by combination of five Gaussian-shaped bands (D4, D3,  
116 D2, D1, and G) following Sadezky et al. [21] and as described in the supple-  
117 mental material (Section S-10.1). The mean crystal size in the  $a$ -direction  
118 ( $L_a$ ) with the fitting constants  $C_0 = -12.6 \text{ nm}$  and  $C_1 = 0.033$ , which are valid

119 for the laser wavelength from 400 to 700 nm, is given by [22]:

$$L_a = \frac{C_0 + C_1 \lambda_L}{A_{D1}/A_G} \quad (1)$$

120 *Thermogravimetric analysis.* The reactivity of soot samples in 20 % volume  
121 fraction CO<sub>2</sub> was determined using a thermogravimetric instrument Q5000  
122 (TA Instrument, USA) by loading ca. 8 mg of sample in an Al<sub>2</sub>O<sub>3</sub> crucible  
123 and heating from 30 to 1200°C in CO<sub>2</sub> at a constant heating rate of 10°C  
124 min<sup>-1</sup>. The kinetic parameters of soot samples were derived by the integral  
125 method presented by Coats and Redfern [23]. The reactivities of biomass  
126 soot samples were compared using reaction rates calculated from the derived  
127 kinetic parameters (A and E<sub>a</sub>) at a fixed gasification temperature of 1000°C.

128 <sup>13</sup>C *solid state NMR spectroscopy.* Solid-state NMR analysis was carried out  
129 on a Nuclear Magnetic Resonance spectrometer, Avance 400 (Bruker, Ger-  
130 many) (9.4 T) operating at Larmor frequencies of 400.13 and 100.58 MHz for  
131 <sup>1</sup>H and <sup>13</sup>C, respectively. All experiments were conducted using a double  
132 resonance probe equipped with 4 mm (o.d.) rotors. Samples were analyzed  
133 without any additional preparation at room temperature by single-pulse (SP)  
134 magic angle spinning (MAS) as well as cross polarization (CP) MAS [24]  
135 utilizing high-power <sup>1</sup>H two-pulse phase-modulated decoupling (TPPM) [25]  
136 during acquisition and employing a spinning rate of 9 kHz. The <sup>13</sup>C CP/MAS  
137 spectra were recorded using a recycle delay of 8 s, a contact time of 1 ms, an  
138 acquisition time of 45.9 ms and 4096 scans, whereas the <sup>13</sup>C SP/MAS spectra  
139 were recorded using a recycle delay of 128 s, an acquisition time of 45.9 ms and  
140 1080 scans. All <sup>13</sup>C NMR spectra were referenced to the carbonyl resonance  
141 in an external sample of α-glycine at 176.5 ppm [26].



142 *X-ray photoelectron spectroscopy.* The XPS spectra were collected with an  
143 electron spectrometer AXIS Ultra DLD (Kratos Analytical Ltd, UK) using  
144 monochromated Al  $K_{\alpha}$  source operated at 120 W. Analyser pass energy of  
145 160 eV for acquiring survey spectra and a pass energy of 20 eV for individual  
146 photoelectron lines were used. The surface potential of dielectric potassium  
147 benzoate was stabilized by the spectrometer charge neutralization system.  
148 The C 1s component for benzene ring ( $sp^2$  carbon) of potassium benzoate  
149 sample was set to aromatic C-H at 284.7 eV [27]. The binding energy scale  
150 of the spectrometer was calibrated using Au  $4f_{7/2}$  line of metallic gold at  
151 84.0 eV. Processing of the spectra was accomplished with the Vision 2 soft-  
152 ware (Kratos Analytical Ltd, UK).

### 153 **3. Results**

#### 154 *3.1. Solubility of potassium in char and soot from herbaceous biomass*

155 Preliminary investigations showed that the ash content of pinewood and  
156 beechwood soot samples remained unchanged after the washing in deionized  
157 water [20]. However, the removal of water-soluble potassium from herbaceous  
158 biomass soot led to a lower reactivity in  $CO_2$  gasification. Figure S-7 illus-  
159 trates that the washing of soot and char from alfalfa straw and wheat straw  
160 does not remove all potassium found in any of the soot samples formed under  
161 fast pyrolysis conditions. The relatively small fraction of potassium remain-  
162 ing in the washed soot from alfalfa and wheat straw suggests the formation  
163 of the potassium-carbon complexes or remaining non-soluble potassium frac-  
164 tion.

165 3.2. Reactivity of biomass soot

166 Figure 1 shows differential weight loss curves (DTG) for the 20% volume  
167 fraction CO<sub>2</sub> gasification of soot samples.

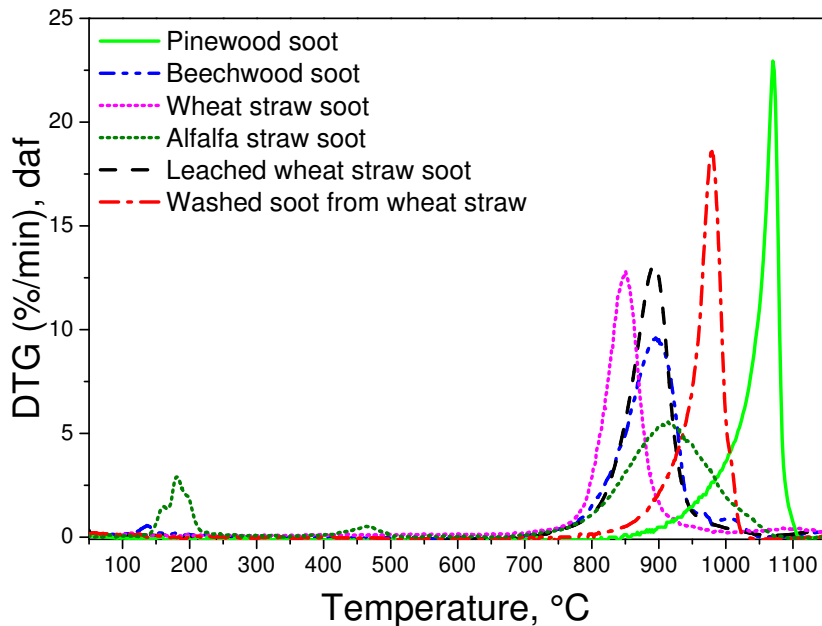


Figure 1: DTG curves of pinewood, beechwood, wheat straw, leached wheat straw, alfalfa straw soot and washed soot from wheat straw reacted in (20% volume fraction CO<sub>2</sub> + 80% volume fraction N<sub>2</sub>). The leached wheat straw soot is soot from wheat straw that was leached in deionized water prior to pyrolysis. The washed soot from wheat straw was prepared by washing soot from original wheat straw in deionized water.

168 The DTG curves show a single broad peak in CO<sub>2</sub> gasification, indicat-  
169 ing a heterogeneous soot mixture with respect to the composition [28]. The  
170 CO<sub>2</sub> gasification of all soot except pine and washed soot from wheat straw  
171 took place at nearly the same temperature range from 850 to 900°C. The

172 additional DTG peaks in the CO<sub>2</sub> gasification of alfalfa straw soot were re-  
173 lated to the reactivity of heavy hydrocarbon compounds [29]. The maximum  
174 reaction rate of pinewood soot was about 200°C higher than for the other  
175 biomasses, and thus, the pinewood soot was clearly less reactive. The wash-  
176 ing of wheat straw soot led to a lower reactivity. The maximum reaction  
177 rate of washed soot of wheat straw in the CO<sub>2</sub> gasification was shifted to  
178 temperatures about 100°C higher than for the soot from pyrolysis of leached  
179 wheat straw and non-treated wheat straw. The calculated  $r_{max}/r_{diff}$  ratio  
180 showed that the gasification reaction in the TG analysis was influenced only  
181 by chemical kinetic limitations, as shown in the supplemental material (Table  
182 S-3).

### 183 3.3. <sup>13</sup>C solid state NMR spectroscopy

184 By <sup>13</sup>C solid-state MAS NMR it was demonstrated that all soot sam-  
185 ples were characterized by a predominantly graphene-like structure [30], as  
186 shown in the supplemental material (Figure S-9). Only in alfalfa straw soot  
187 an additional presence of a carboxylate carbon was detected. The chemi-  
188 cal shift of this agrees well with that of the potassium-calcium carbonate  
189 butschliite [31–33].

### 190 3.4. X-ray photoelectron spectroscopy

191 The XPS spectra of pinewood and beechwood soot mainly exhibit the  
192 carbon and oxygen lines with some traces of sodium, whereas herbaceous  
193 biomass soot samples additionally showed K 2p and Cl 2p lines, as shown in  
194 the supplemental material (Table S-4). The K and Cl atomic concentrations  
195 for the alfalfa straw soot were 3.5 and 1.2 at. %, whereas the K and Cl atomic

196 ratio in pure KCl is 1:1, respectively. The remaining potassium (2.3 at. %)   
197 might have been bounded to the soot matrix as KOH and/or  $K_2CO_3$  which   
198 was not detected (or fitted) in C 1s spectrum due to small amounts. The   
199 present XPS results strongly suggest that potassium species were incorpo-   
200 rated in straw soot particles mostly as water-soluble KCl,  $K_2CO_3$  and KOH.

### 201 3.5. Raman spectroscopy

202 Raman spectroscopy was carried out to examine primary differences in   
203 the carbon structure of soot samples. The calculated integrated peak area   
204 ratio ( $A_{D4}/A_G$ ) in supplementary Table S-5 showed that the beechwood and   
205 leached wheat straw soot samples obtained the highest amount of carboxy-   
206 lates (0.2 and 0.3), whereas the  $A_{D4}/A_G$  ratio of wheat straw soot was the   
207 lowest (0.04). The relative  $A_{D4}/A_G$  ratio of pinewood soot is lower than   
208 for beechwood soot due to the low content of acetyl groups in hemicellulosic   
209 fraction of softwood [34]. All soot samples based on the  $A_{D1}/A_G$  ratios exhib-   
210 ited a common structure of amorphous carbon and nano-crystalline graphite,   
211 as discussed by Ferrari and Robertson [35]. In addition, the alfalfa straw   
212 soot contained a higher fraction of distorted small PAH clusters within the   
213 amorphous carbon than other soot samples, as observed experimentally by   
214 Abboud et al. [36]. The average extensions of graphene stacks ( $L_a$ ) from the   
215 Raman bands in beechwood, wheat straw, alfalfa straw and leached wheat   
216 straw soot were lower than those of pinewood and washed soot from wheat   
217 straw. The size of one aromatic ring is 2.5 Å [37], and therefore, the size of   
218 PAHs ( $L_a = 21\text{-}26$  Å) is equivalent to the size of 8-10 aromatic rings.

219 *3.6. X-ray diffraction*

220 The XRD analysis did not show any significant differences between  
221 woody and herbaceous soot samples in terms of graphitization, as shown  
222 in the supplemental material (Figure S-41). The XRD analysis of soot in-  
223 dicated formation of turbostratic or random layer lattice structures. The  
224 additional reflections, detected by the XRD measurements of wheat straw  
225 and alfalfa straw soot, were attributed to KCl and  $\text{KHCO}_3$ .

226 **4. Discussion**

227 The thermogravimetric experiments demonstrated significant differences  
228 in  $\text{CO}_2$  reactivity for soot from pyrolysis of wood and herbaceous biomass.  
229 The  $\text{CO}_2$  gasification of beechwood, wheat straw, alfalfa straw and leached  
230 wheat straw soot prepared at  $1250^\circ\text{C}$  took place at nearly the same tem-  
231 perature range, whereas the maximum reaction rate of pinewood soot and  
232 washed soot from wheat straw was shifted to higher temperatures, indicating  
233 a lower reactivity.

234 The reactivity of soot samples can be affected by the differences in car-  
235 bon structure and alkali content [6, 38, 39]. Lapuerta et al. [40] studied soot  
236 samples generated from the combustion of biodiesel and diesel fuels using  
237 thermogravimetric analysis and Raman spectroscopy and the authors found  
238 that the impact of soot nanostructure on the oxidation reactivity is signifi-  
239 cant. The biodiesel soot has a higher initial degree of graphitization with the  
240 higher curvature of the carbon fringes of an average particle size which in-  
241 creases the probability of collapsing into smaller fringes, and thus, enhances  
242 the reactivity. Trubetskaya et al. [41] studied the impact of lignocellulosic

243 compounds and monolignols on the biomass soot reactivity and showed that  
244 the high content of extractives and lignin in the pinewood and beechwood  
245 could lead to the lower reactivity of woody soot. The previous studies also  
246 showed that the maximal reaction rates of extractives and lignin soot sam-  
247 ples were less reactive than the cellulose and hemicellulose soot, emphasizing  
248 a dominating role of differences in lignocellulosic composition on the soot  
249 reactivity. Interestingly, the authors found that the CO<sub>2</sub> reactivities of soft-  
250 wood and wheat straw lignin soot were similar beside the fact that the low  
251 ash-containing softwood lignin soot was expected to be less reactive than  
252 the Na<sup>+</sup> rich wheat straw lignin soot. In the present study, the Raman  
253 spectroscopy analysis showed that the alfalfa straw soot consists of small  
254 PAH clusters within the amorphous carbon with high curvatures of carbon  
255 fringes forming higher specific surface area, leading to the higher reactivity.  
256 In addition, the alfalfa and wheat straw soot samples obtained the highest  
257  $A_D/A_G$  ratio. Thus, more defective graphene sheets could form smaller car-  
258 bon segments with a higher specific surface area resulting in the high CO<sub>2</sub>  
259 reactivity. This indicates that the carbon structure has an influence on the  
260 observed differences in soot reactivity. In addition, the previous Raman spec-  
261 troscopy analysis indicated that the differences in carbon structure of soot  
262 from holocelluloses, lignin and monolignols were small [41]. However, the ash-  
263 forming elements are known to influence both the shape and nanostructure of  
264 pinewood soot particles during the entrained flow gasification of biomass [6].  
265 In the present work, the Raman spectroscopy results suggested that the re-  
266 leased alkali metal ions in the biomass pyrolysis had an influence on the soot  
267 carbon structure, leading to the formation of defects in the carbon matrix.

268 Previous results showed that the soot CO<sub>2</sub> reactivity depends mainly  
269 on the alkali content in the original fuel and less on the soot nanostructure  
270 and soot particle size [42]. For the Ca and Na rich biodiesel soot, higher ox-  
271 idation reactivities were observed than for the low ash-containing farnesane  
272 and diesel soot samples [43]. The authors also indicated that Ca, Na, and P  
273 compounds had a dominant role on the soot reactivity compared to the dif-  
274 ferences in nanostructure of biodiesel and diesel soot samples. Gustafsson et  
275 al. [44] observed that Ca was a dominant ash-forming element in wood pellet  
276 combustion. In the present study, the ash content in the original beech-  
277 wood (1.4 %) was higher than in the pinewood (0.3 %), leading to the higher  
278 K release to the gas phase and so more K incorporation in the beechwood  
279 soot particles compared to the pinewood pyrolysis. The ash content in the  
280 original alfalfa straw (7.2 %) was also higher than in the non-treated wheat  
281 straw (4.1 %) and leached wheat straw (2.1 %). The inorganic elements in  
282 all herbaceous biomass soot samples were mainly K, Cl, S, and Si. Previ-  
283 ous equilibrium calculations and X-ray diffraction reflections suggested an  
284 incorporation of water-soluble KCl in the alfalfa, non-treated and leached  
285 wheat straw soot samples [45]. The present results showed that 50 % more  
286 of potassium was condensed onto the leached wheat straw soot compared to  
287 the non-treated wheat straw soot where potassium was probably retained as  
288 a silicate in the char. The lower Cl content in the leached wheat straw might  
289 indicate that potassium was released in the form of KOH, possibly forming  
290 K<sub>2</sub>CO<sub>3</sub> [46]. Based on the XRD and XPS analysis results it was concluded  
291 that the potassium species were incorporated in the alfalfa and wheat straw  
292 soot particles mostly as KOH, KCl, KHCO<sub>3</sub> and K<sub>2</sub>CO<sub>3</sub>. The present results

293 showed that potassium compounds represent major alkali metal ions incor-  
294 porated into the biomass soot matrix. In addition, the XPS results showed  
295 that the elemental potassium was not bonded to the soot matrix in phenolate  
296 groups and was mainly adsorbed as potassium hydroxide and/or potassium  
297 carbonate on the herbaceous soot particle surfaces which is probably due  
298 to the short contact time in high-temperature biomass pyrolysis. The XPS  
299 results also indicated that the alkali metal compounds were not detected for  
300 pinewood soot.

301       The water-soluble salts affect the biomass soot reactivity [42]. Soot from  
302 alfalfa straw, wheat straw, beechwood and leached wheat straw was 14 times  
303 more reactive than pinewood soot and washed soot from wheat straw, due  
304 to the stronger catalytic effect of ash compounds. Significantly smaller dif-  
305 ferences in CO<sub>2</sub> reactivity were observed for the pinewood soot and washed  
306 soot from wheat straw (2 times), as shown in the supplemental material (Ta-  
307 ble S-2). The amount and composition of the ash forming matter in the  
308 lignocellulosic materials lead to the differences in soot reactivity. The potas-  
309 sium content of leached wheat straw soot was lower than for alfalfa straw  
310 and wheat straw soot, and higher than for beechwood soot. However, the  
311 differences in reactivity of soot from beechwood, wheat straw, alfalfa straw  
312 and leached wheat straw were small, as shown in Figure 2. The remaining  
313 potassium compounds in the washed soot from wheat straw led to a slightly  
314 higher reactivity compared to the pinewood soot. Thus, the present study in-  
315 dicated that the water-soluble salts determine the catalytic gasification rate  
316 because electron donor-acceptor (EDA) complexes and C-O-K groups on the  
317 soot surface were not formed. The high reactivity of potassium rich herba-



318 ceous soot samples was related to the reduction-oxidation cycles of  $K_2CO_3$ ,  
 319 elemental potassium, and  $K_2O$  according to equations 2-4 [47, 48]:

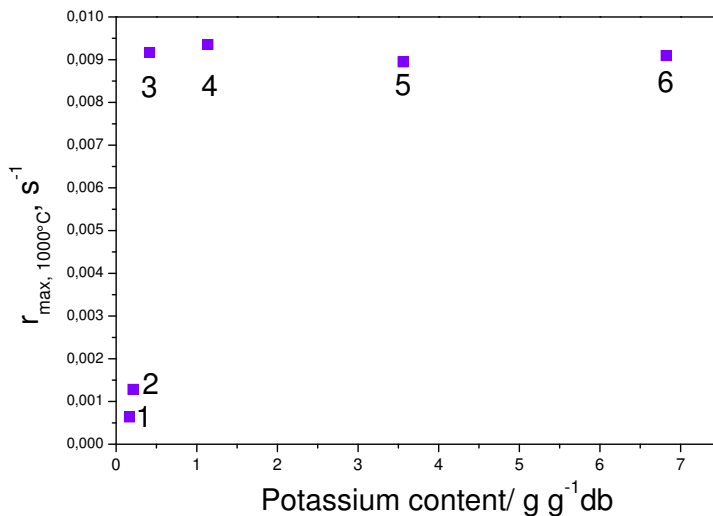
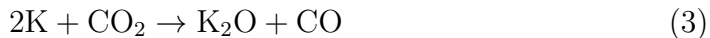


Figure 2: Maximal reaction rate at  $1000^\circ C$  (results from Table S-2) versus potassium content in soot from pinewood, beechwood wheat straw, alfalfa straw, leached wheat straw and washed soot from wheat straw (results from Figures S-5, S-6, S-7). The potassium content is shown in wt. % relative to the soot ( $g\ g^{-1}$  on dry basis).

320 In addition, the catalytic effect of potassium on the reactivity remained  
 321 similar after a certain concentration of potassium is reached in the soot parti-  
 322 cles, and thus, the changes in reactivity of soot from pyrolysis of alfalfa straw,

323 wheat straw and leached wheat straw were small. The removal of potassium  
324 from the original wheat straw does not affect the soot reactivity. In contrast,  
325 the estimated activation energy of wheat straw soot increased from 209 to  
326 225 kJ mol<sup>-1</sup> after the washing in deionized water as shown in the supple-  
327 mental material (Table S-2), indicating that the removal of potassium leads  
328 to a lower soot reactivity. Figure 2 shows that the reactivity of soot sam-  
329 ples generated from dry feedstocks with potassium concentration > 0.3 wt.%  
330 changed only slightly. The contact between alkali metals and carbon is an  
331 essential parameter in the catalytic gasification of biomass that can be im-  
332 proved by mobility of the alkali metals [49]. The present results showed that  
333 the K<sub>2</sub>CO<sub>3</sub> had a good contact with the soot carbonaceous matrix, leading  
334 to the higher CO<sub>2</sub> reactivity with the increased content of potassium until  
335 saturation was reached.

## 336 5. Conclusion

337 The novelty of this work relies on the fact that potassium is unlikely  
338 to be bonded to oxygen-containing surface groups in the soot matrix dur-  
339 ing high temperature pyrolysis. The present results showed that potassium  
340 was deposited on the soot surface as water-soluble alkali such as KCl, KOH,  
341 KHCO<sub>3</sub> and K<sub>2</sub>CO<sub>3</sub>. The thermogravimetric analysis showed that the differ-  
342 ences in CO<sub>2</sub> reactivity are large for soot from wood and herbaceous biomass  
343 pyrolysis. The CO<sub>2</sub> reactivity of soot depends mainly on the potassium con-  
344 tent in the original fuel and less on the carbon chemistry. However, the  
345 catalytic effect of potassium on the reactivity remains the same after a cer-  
346 tain potassium amount was deposited on the surface of soot particles during

347 pyrolysis. The low ash containing pinewood soot was less reactive with the  
348 more ordered graphene structure than other soot samples. The carbon struc-  
349 ture of alfalfa and wheat straw soot appeared more graphitic disordered and  
350 contributed to the greater reactivity in CO<sub>2</sub> gasification. The present work  
351 emphasized a significant influence of both potassium and carbon structure  
352 on the biomass soot reactivity.

### 353 **Acknowledgements**

354 The authors gratefully acknowledge financial support from the Kempe  
355 Foundation, the Swedish Energy Agency and the Swedish strategic research  
356 program Bio4Energy. The authors acknowledge the facilities and technical  
357 support of Dr. Nikki Lee of the Umeå Core Facility for Electron Microscopy  
358 (UCEM) at the Chemical and Biological Centre (KBC), Dr. Andras Gorzsas,  
359 Dr. Nils Skoglund and Dr. Markus Broström at Umeå University. We ac-  
360 knowledge Avery Brown from Worcester Polytechnic Institute for the article  
361 proof-reading.

### 362 **References**

- 363 [1] Carlsson P, Ma C, Molinder R, Weiland F, Wiinikka H, Öhman M and  
364 etc., Slag formation during oxygen-blown entrained-flow gasification of  
365 stem wood, *Energy Fuels* 28 (2014) 6941–52.
- 366 [2] Ma C, Backman R, Öhman M, Thermochemical Equilibrium Study  
367 of Slag Formation during Pressurized Entrained-Flow Gasification of  
368 Woody Biomass, *Energy Fuels* 29 (2015) 4399–406.

- 369 [3] Chen SG, Yang RT, The Active Surface Species in Alkali-Catalyzed Car-  
370 bon Gasification: Phenolate (C-O-M) Groups vs Clusters (Particles), J  
371 Catalysis 141 (1993) 102–13.
- 372 [4] Septien S, Valin S, Peyrot M, Dupont C, Salvador S, Characterization  
373 of char and soot from millimetric wood particles pyrolysis in a drop tube  
374 reactor between 800°C and 1400°C, Fuel 121 (2014) 216–24.
- 375 [5] Akuzawa N, Yoshioka J, Ozaki C, Tokuda M, Ohkura K, Soneda Y,  
376 Preparation and characterization of sodium-graphite intercalation com-  
377 pounds, Mol Cryst Liq Cryst 388 (1) (2002) 1–7.
- 378 [6] Wiinikka H, Weiland F, Pettersson E, Öhrman O, Carlsson P, Stjern-  
379 berg J, Characterization of submicron particles produced during oxygen  
380 blown entrained flow gasification of biomass, Combust Flame 161 (2014)  
381 1923–34.
- 382 [7] Kopyscinski J, Rahman M, Gupta R, Mims CA, Hill JM,  $K_2CO_3$  cat-  
383 alyzed  $CO_2$  gasification of ash-free coal. Interactions of the catalyst with  
384 carbon in  $N_2$  and  $CO_2$  atmosphere, Fuel 117 (2014) 1181–9.
- 385 [8] Wen YW, Mechanisms of Alkali Metal Catalysis in the Gasification of  
386 Coal, Char, or Graphite, Cat Rev Sci Eng 22 (1) (1980) 1–28.
- 387 [9] Sekhar MVC, Ternan M, Catalytic gasification of char from hydroc-  
388 racked pitch, Fuel Process Tech 6 (1982) 61–73.
- 389 [10] Wigmans T, Elfring R, Moulijn JA, On the mechanism of the potassium  
390 carbonate catalysed gasification of activated carbon: The influence of

- 391 the catalyst concentration on the reactivity and selectivity at low steam  
392 pressures, Carbon 21 (1) (1983) 1–12.
- 393 [11] Dresselhaus MS, Dresselhaus G, Eklund PC, Science of fullerenes and  
394 carbon nanotubes, Academ Press, 1996.
- 395 [12] Winter J, Kuzmany H, Physical properties and phase transitions in  
396 AC(60), Carbon 36 (5-6) (1998) 599–601.
- 397 [13] Tycko R, Molecular orientational dynamics in solid C-70 investigation  
398 by one-dimensional and 2-dimensional magic-angle-spinning nuclear-  
399 magnetic-resonance, J Phys Chem Solids 54 (12) (1993) 1713–23.
- 400 [14] Gunnarsson O, Superconductivity in fullerenes, Carbon 69 (2) (1997)  
401 575–606.
- 402 [15] Skokan EV, Tarasov VP, Privalov VI, Aleshina VE, Muravlev YB,  
403 Arkhangelskii IV, Intercalation of potassium into fullerite C<sub>60</sub>: <sup>13</sup>C and  
404 <sup>39</sup>K NMR data, Electrochem Soc Proc 15 (2003) 509–14.
- 405 [16] Chun KY, Controlling the doping level of double-walled carbon nan-  
406 otubes by using aromatic hydrocarbon complexes, RSC Adv 4 (2014)  
407 8879–82.
- 408 [17] Caballero A, Adsorption and oxidation of K deposited on graphite, Surf  
409 Sci 364 (1996) 253–65.
- 410 [18] Li Q, Wang X, Xin Y, Zhang Z, Zhang Y, Hao C and etc., A unified in-  
411 termediate and mechanism for soot combustion on potassium-supported  
412 oxides, Sci Rep 4 (2014) 4725–31.

- 413 [19] Mejer R, Weeda M, Kapteijn F, Moulijn JA, Catalyst loss and retention  
414 during alkali-catalyzed carbon gasification in CO<sub>2</sub>, Carbon 29 (7) (1991)  
415 929–41.
- 416 [20] Trubetskaya A, Jensen PA, Jensen AD, Garcia Llamas AD, Umeki K,  
417 Glarborg P, Effect of fast pyrolysis conditions on biomass solid residues  
418 at high temperatures, Fuel Process Tech 143 (2016) 118–29.
- 419 [21] Sadezky A, Muckenhuber H, Grothe H, Niessner R, Pöschl U, Raman  
420 spectroscopy of soot and related carbonaceous materials: Spectral anal-  
421 ysis and structural information, Carbon 43 (2005) 1731–42.
- 422 [22] Matthews MJ, Pimenta MA, Dresselhaus G, Origin of dispersive effects  
423 of the Raman D band in carbon materials, Phys Rev B 59 (10) (1999)  
424 R6585–88.
- 425 [23] Coats AW, Redfern JP, Kinetic Parameters from Thermogravimetric  
426 Data, Nature 201 (1964) 68–9.
- 427 [24] Peersen OB, Wu X, Kustanovich I, Smith SO, Variable-Amplitude  
428 Cross-Polarization MAS NMR, J Magn Reson Ser A 104 (3) (1993)  
429 334–9.
- 430 [25] Bennett AE, Rienstra CM, Auger M, Lakshmi KV, Griffin RG, Het-  
431 eronuclear decoupling in rotating solids, J Chem Phy 103 (1995) 6951–8.
- 432 [26] Potrzebowski MJ, Tekely P, Dusausoy Y, Comment to <sup>13</sup>C NMR studies  
433 of alpha and gamma polymorphs of glycine, Solid State Nucl Magn  
434 Reson 11 (3-4) (1998) 253–7.

- 435 [27] Beamson G, Briggs D, The XPS of Polymers Database. CD Version 1.0.,  
436 SurfaceSpectra Ltd, 2000.
- 437 [28] Russell NV, Beeley TJ, Man CK, Gibbins JR, Williamson J, Develop-  
438 ment of TG measurements of intrinsic char combustion reactivity for  
439 industrial and research purposes, Fuel Process Tech 57 (2) (1998) 113–  
440 30.
- 441 [29] Zhang D, Ma Y, Zhu M, Nanostructure and oxidative properties of soot  
442 from a compression ignition engine: The effect of a homogeneous com-  
443 bustion catalyst, Proc Combust Inst 34 (2013) 1869–76.
- 444 [30] Freitas JCC, Emmerich FG, Bonagamba TJ, High-Resolution Solid-  
445 State NMR Study of the Occurrence and Thermal Transformations of  
446 Silicon-Containing Species in Biomass Materials, Chem Mater 12 (3)  
447 (2000) 711–8.
- 448 [31] Papenguth HW, Kirkpatrick RJ, Montez B, Sandberg PA,  $^{13}\text{C}$  MAS  
449 NMR spectroscopy of inorganic and biogenic carbonates, Am Miner 74  
450 (1989) 1152–8.
- 451 [32] Stueber D, Patterson D, Maybe CL, Orendt AM, Grant DM, Parry RW,  
452 Carbonates, Thiocarbonates, and the Corresponding Monoalkyl Deriva-  
453 tives. 1. Their Preparation and Isotropic  $^{13}\text{C}$  NMR Chemical Shifts,  
454 Inorg Chem 40 (2001) 1902–11.
- 455 [33] Shatskiy A, Borzdov YM, Litasov KD, Sharygin IS, Palyanov YN,  
456 Ohtani E, Phase relationship in the system  $\text{K}_2\text{CO}_3\text{-CaCO}_3$ , Fuel 117  
457 (2014) 1181–9.

- 458 [34] Sun Y, Cheng J, Hydrolysis of lignocellulosic materials for ethanol pro-  
459 duction: a review, *Biores Tech* 83 (2002) 1–11.
- 460 [35] Ferrari AC, Robertson J, Raman spectroscopy of amorphous, nanostruc-  
461 tured, diamond-like carbon, and nanodiamond, *Phil Trans R Soc Lond*  
462 362 (2004) 2477–512.
- 463 [36] Abboud J, Schobing J, Legros G, Bonnety J, Tschamber V, Brillard  
464 A and etc., Impacts of oxygenated compounds cocentration on sooting  
465 propensities and soot oxidative reactivity: Application to Diesel and  
466 Biodiesel surrogates, *Fuel* 193 (2017) 241–53.
- 467 [37] Hayashida K, Nagaoka S, Ishitani H, Growth and oxidation of graphitic  
468 crystallites in soot particles within a laminar diffusion flame, *Fuel* 128  
469 (2014) 148–54.
- 470 [38] Müller JO, Investigations on Environmental Carbons. PhD thesis, Tech-  
471 nical University of Berlin, 2012.
- 472 [39] Liati A, Eggenschwiler PD, Schreiber D, Zelenay V, Ammann M, Varia-  
473 tions in diesel soot reactivity along the exhaust after-treatment system,  
474 based on the morphology and nanostructure of primary soot particles,  
475 *Combust Flame* 160 (3) (2013) 671–81.
- 476 [40] Lapuerta M, Oliva F, Agudelo JR, Boehman AL, Effect of fuel on the  
477 soot nanostructure and consequences on loading and regeneration of  
478 diesel particulate filters, *Combust Flame* 159 (2012) 844–53.
- 479 [41] Trubetskaya A, Brown A, Tompsett GA, Timko MT, Umeki K, Kling J  
480 and etc., Characterization and reactivity of soot from fast pyrolysis of



- 481 lignocellulosic compounds and monolignols, *Applied Energy* 212 (2018)  
482 1489–500.
- 483 [42] Trubetskaya A, Jensen PA, Jensen AD, Garcia Llamas AD, Umeki K,  
484 Kling J and etc., Effects of several types of biomass fuels on the yield,  
485 nanostructure and reactivity of soot from fast pyrolysis at high temper-  
486 atures, *Applied Energy* 171 (2016) 468–82.
- 487 [43] Soriano JA, Agudelo JR, Lopez AF, Armas O, Oxidation reactivity and  
488 nanostructural characterization of the soot coming from farnesane - A  
489 novel diesel fuel derived from sugar cane, *Carbon* 125 (2017) 516–29.
- 490 [44] Gustafsson E, Strand M, Sanati M, Physical and Chemical Characteriza-  
491 tion of Aerosol Particles Formed during the Thermochemical Conversion  
492 of Wood Pellets Using a Bubbling Fluidized Bed Gasifier, *Energy Fuels*  
493 21 (2007) 3660–7.
- 494 [45] Trubetskaya A, Jensen PA, Jensen AD, Steibel M, Spliethoff H, Glarborg  
495 P, Hofmann Larsen F, Comparison of the high temperature chars of  
496 wheat straw and rice husk with respect to chemistry, morphology and  
497 reactivity, *Biomass Bioenergy* 86 (2016) 76–87.
- 498 [46] Dayton DC, Milne TA, Laboratory Measurements of Alkali Metal Con-  
499 taining Vapors Released during Biomass Combustion. In: Baxter L. and  
500 DeSollar R. (ed.), *Applications of Advanced Technology to Ash-Related*  
501 *Problems in Boilers*, Plenum Press, 1996.

- 502 [47] Miro EE, Ravelli F, Ulla MA, Cornaglia LM, Querini CA, Catalytic  
503 combustion of diesel soot on Co, K supported catalysts, Catal Today  
504 53 (4) (1999) 631–8.
- 505 [48] Neeft PA, Makkee M, Moulijn JA, Catalytic oxidation of carbon black -  
506 I. Activity of catalysts and classification of oxidation profiles, Fuel 77 (3)  
507 (1998) 111–9.
- 508 [49] Neeft PA, Makkee M, Moulijn JA, Catalysts for the oxidation of soot  
509 from diesel exhaust gases. I. An exploratory study, Appl Catal B: Env-  
510 iron 8 (1) (1996) 57–78.